AIChE

Decomposition Kinetics and Recycle of Binary Hydrogen-Tetrahydrofuran Clathrate Hydrate

Hiroki Yoshioka, Masaki Ota, Yoshiyuki Sato, Masaru Watanabe, Hiroshi Inomata, and Richard L. Smith Jr.
Research Center of Supercritical Fluid Technology, Tohoku University, Aramaki Aza, Aoba-ku, Sendai 980-8579, Japan

Cor J. Peters
Laboratory of Process Equipment, Dept. of Process and Energy, Faculty of Mechanical, Maritime and Materials Engineering, Delft University of Technology, 2628 CA Delft, The Netherlands; Petroleum Institute, Chemical Engineering Program, Abu Dhabi, United Arab Emirates

DOI 10.1002/aic.12241
Published online August 12, 2010 in Wiley Online Library (wileyonlinelibrary.com).

Decomposition kinetics and recycle of hydrogen–tetrahydrofuran (H_2–THF) clathrate hydrates were investigated with a pressure decay method at temperatures from 265.1 to 273.2 K, at initial pressures from 3.1 to 8.0 MPa, and at stoichiometric THF hydrate concentrations for particle sizes between 250 and 1000 μm. The decomposition was modeled as a two-step process consisting of H_2 diffusion in the hydrate phase and desorption from the hydrate cage. The adsorption process occurred at roughly two to three times faster than the desorption process, whereas the diffusion process during formation was slightly higher (ca. 20%) than that during decomposition. Successive formation and decomposition cycles showed that occupancy seemed to decrease only slightly with cycling and that there were no large changes in hydrate structure due to cycling. Results provide evidence that the formation and decomposition of H_2 clathrate hydrates occur reversibly and that H_2 clathrate hydrates can be recycled with pressure. © 2010 American Institute of Chemical Engineers *AIChE J,* 57: 265–272, 2011

Keywords: hydrogen storage, clathrate hydrate, formation kinetics, hydrogen hydrate phase diffusion model

Introduction

The potential of tetrahydrofuran (THF) clathrate hydrates for hydrogen (H_2) storage continues to be of interest, where it has been demonstrated with precise measurements that THF hydrate can store up to 1.6 mol H_2/mol THF (0.045 g H_2/g THF) at 277.15 K and 70 MPa.[1] Moreover, there is the possibility for using other guest molecules[2,3] or hybrid structures[4] that could allow achievement of greater H_2 storage capacities, since current storage capacity is considered to be low for practical applications.[5]

However, in considering the storage capacity of H_2 in a clathrate hydrate structure, not only formation kinetics but also release or decomposition kinetics of the clathrate hydrate are important for practical use. A number of authors have indicated that storage and release of H_2 can be performed without destroying the hydrate cages and some have presented data showing the decomposition of the clathrate to recover H_2,[6,7] but these studies lack quantitative description of the macroscopic physical and chemical processes occurring that are shown by the time variation of experimental

Additional Supporting Information may be found in the online version of this article.

Correspondence concerning this article should be addressed to R. L. Smith at smith@scf.che.tohoku.ac.jp.

Table 1. Experimental Conditions Used to Study Formation and Decomposition of Hydrogen–Tetrahydrofuran Clathrate Hydrates

Run	W_{Hyd} (g)	A (cm^2)	T (K)	P (f) (MPa)	d (μm)
1	7.32	8.22×10^{-2}	269.0	5.0 (5.2)	500–600
2	4.02	8.20×10^{-2}	269.1	5.0 (5.1)	250–355
3	12.4	8.22×10^{-2}	269.0	5.0 (5.2)	850–1000
4	7.31	8.21×10^{-2}	269.2	8.0 (8.4)	500–600
5	7.27	8.17×10^{-2}	269.2	3.1 (3.1)	500–600
6	7.30	8.20×10^{-2}	273.2	5.0 (5.2)	500–600
7	7.36	8.26×10^{-2}	265.1	5.0 (5.2)	500–600
8	7.30	8.20×10^{-2}	269.1	5.0 (5.2)	500–600

W_{Hyd}, total mass of hydrate used; A, total surface area of hydrate used; T, experimental temperature; $P(f)$, experimental pressure and fugacity; d, sieved range of hydrate particles.

data in the bulk phase. Several researchers have investigated kinetics focusing on diffusion of H_2 or deuterium in clathrate hydrates[8–12] and give evidence for the microscopic adsorption and diffusional processes that should be included in formulating a phenomenological model. Some models that have been proposed include additional effects such as lattice distortion,[13,14] while others have analyzed equilibrium conditions for H_2 occupancy by Monte Carlo simulation[15] and molecular dynamics (MD) simulation.[16] Papadimitriou et al.[17] have proposed changes in the methodology for calculating H_2 occupancy with promoters with the use of equilibrium data.

In a previous study on binary H_2–THF clathrate hydrate formation kinetics, we developed a phenomenological model that assumed hydrate formation via an adsorption step and a subsequent diffusion step.[18] To take into account, the progressive inhibition of inclusion as H_2 clathrate forms, the hydrate phase thickness was assumed to be proportional to the H_2 occupancy at any given time. The hydrogen hydrate phase diffusion (HHPD) model[18] was found to provide good correlation of the experimental results with respect to particle size, temperature, and pressure variations. Nevertheless, that work left open some important questions that need to be addressed, which include the temperature dependence of the formation and decomposition kinetics, the reversibility of the formation process, and the extent to which H_2 stored as binary H_2–THF clathrate hydrates can be recycled or reused.

In this work, we examine formation and decomposition kinetics of binary H_2–THF clathrate hydrates with an apparatus and procedure that were modified to improve both the temperature control and reproducibility of the experiments over previous work. We develop a model that can describe the decomposition kinetics by considering the previous HHPD model and apply the model to study the decomposition process according to temperature, particle size, and pressure variations. Experiments are performed that examine recycle of the binary H_2–THF clathrate hydrates through multiple formation and decomposition cycles of the same clathrate hydrates such that conclusions can be made on the reversibility of the formation and decomposition processes. A modification to the HHPD model is proposed that relates the hydrate phase thickness during desorption to the ratios of differences between H_2 occupancy at formation and that after decomposition. As decomposition of clathrate hydrate also requires formation experiments, additional formation runs are presented in this work with improved temperature control.

Experimental Methods

Materials

Distilled and deionized water was used that had an electrical conductivity of 5.5 μS/m. H_2 gas (99.99%, Iwaki Suiso) and THF without stabilizer (99.5%, Wako Pure Chemical) were used.

Hydrate preparation

Batches of THF clathrate hydrate particles were made by loading water and THF into a perfluoroalkoxyethylene vessel and weighing the contents to a precision of 1 mg with a balance (Mettler Toledo AX504) and then cooling the solution to 253 K with a freezer (Norfrost, HNC100) while stirring. After at least 1 day at 253 K, the solids were crushed with a mortar and pestle at liquid nitrogen temperatures and then graded with stainless steel–type 316 sieves while being kept in the freezer at 253 K. The formation of THF clathrate hydrate was confirmed with laser Raman spectroscopy (JASCO, NR-2000) by comparison with spectra for liquid THF, a 19.06 wt% THF–water solution, and the product THF clathrate hydrate (Supporting Information, Figure S1). Particle size ranges of 250–355 μm, 500–600 μm, and 850–1000 μm were used in the experiments with the actual mass of clathrate hydrate loaded into the cell being adjusted to have a constant surface area of 0.082 m^2 (Table 1). In the formation and decomposition experiments, eight runs were performed that varied temperature, pressure, and particle size range (Table 1). In the recycle experiments, three formation and decomposition runs were performed.

The experimental apparatus (Figure 1) was modified and the procedures used were improved over those used in the previous work on formation kinetics.[18] As shown in Figure 1a, 4-wire Pt thermometers (Netsushin Co.) were added to both hydrate formation cell and to the H_2 reservoir tank. The reservoir tank system (Figure 1b) was designed to be separated from the equilibrium cell during the loading of the reservoir tank with H_2. An additional pressure gauge (Setra, 280E) was added to the reservoir tank system.

The H_2 reservoir tank system (Figure 1b) used two 300 cm^3 sampling bombs (Whitey, 304-HDF4-300) and a cooling unit (Julabo, F-25 MB). The reservoir tank was volume calibrated with nitrogen over the range of temperatures (269–273 K) and pressures (2.5–5.3 MPa) and found to have an average volume of 300.79 cm^3 from seven independent trials ($\sigma = 0.447$ cm^3). The hydrate formation cell was volume

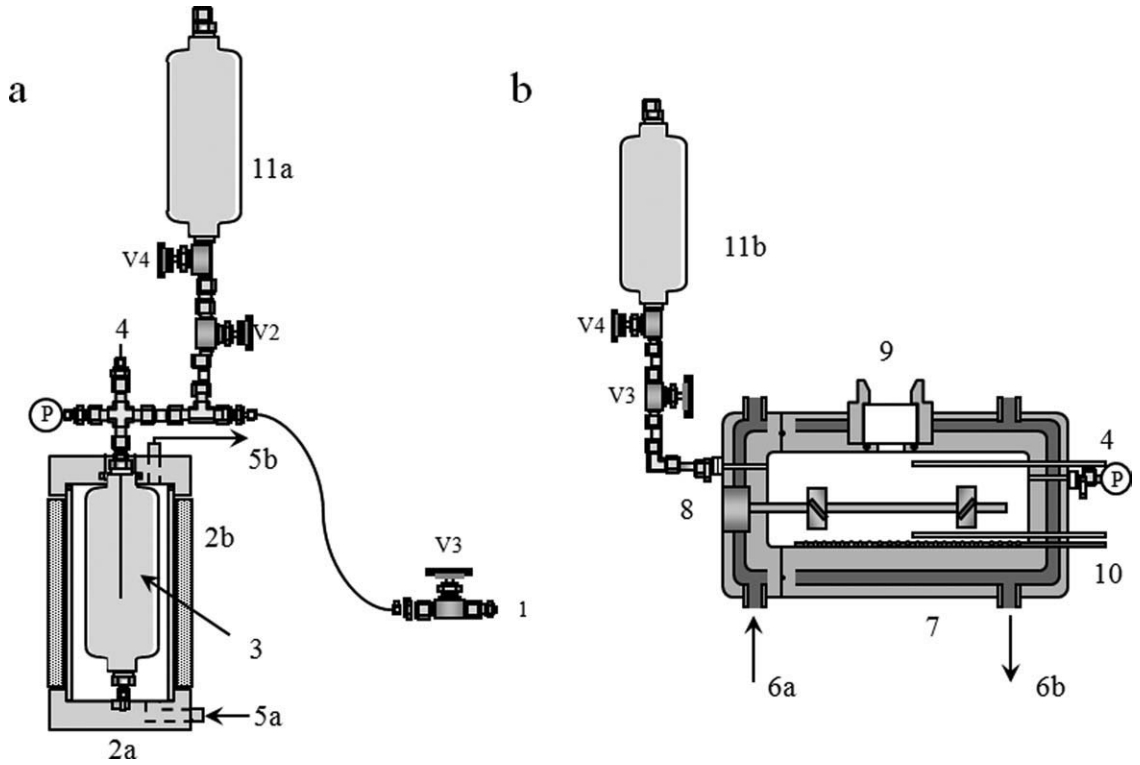

Figure 1. Apparatus used in hydrogen clathrate hydrate formation and decomposition experiments.

(a) H_2 reservoir loading system and (b) hydrate formation cell. Components, 1: connection to H_2 cylinder, 2a: Glycol jacket (hard vinyl chloride), 2b: insulation (AEROFLEX®) 3: reservoir tank, 4: 4-wire Pt thermometers, 5a: chiller inlet, 5b: chiller outlet; 6a: chiller inlet, 6b: chiller outlet, 7: hydrate formation cell, 8: agitator, 9: window, 10: thermocouple (T-type), 11a: transferable sampling bomb connected to reservoir tank, 11b: transferable sampling bomb connected to hydrate formation cell.

calibrated with nitrogen over a range of temperatures (269–273 K) and pressures (2.2–7.4 MPa) and found to have an average volume of 134.75 cm^3 from 12 independent trials (σ = 0.255 cm^3). Temperature control of the reservoir tank was better than 0.1 K that improved the reproducibility of H_2 quantification.

The modified experimental apparatus as described above was used for studies of both formation and decomposition kinetics. The procedure used in the formation experiments was based on the pressure decay method using material balances for H_2 in both the cell and reservoir tank as in the previous work[19] with the exception that the initial surface area of the THF clathrate hydrate was held constant by changing the loaded amounts (Table 1) as indicated earlier. Reproducibility of the H_2 quantification for THF clathrate hydrate formation for a given set of conditions was found to be consistent for two independent runs to within 2.0% during formation for more than 4000 pressure measurement points (Supporting Information, Figure S2a) and to within 1.6% during decomposition for more than 4000 pressure measurement points (Supporting Information, Figure S2b).

The procedure used in the decomposition experiments was as follows: When the hydrate formation cell reached equilibrium conditions, the cell was depressurized rapidly to atmospheric pressure (ca. 0.1 MPa) to remove the gas phase H_2. Once the cell was depressurized, it was immediately isolated and temperature was controlled to the given experimental temperature while the pressure was monitored over a period of time (ca. 8–30 h) as documented in Supporting Information, Figure S3. The amount of H_2 released was calculated from the material balance and an equation of state[20] by dividing the mass of H_2 due to the increase in pressure in the cell by the loaded mass of hydrate particles. Typical variations in pressure, gas phase temperature, and hydrate phase temperature for both the formation and decomposition processes are given in Supporting Information, Figure S3. Raman spectra were taken to confirm the existence of THF hydrate and binary H_2–THF hydrate (Supporting Information, Figure S4).

HHPD model

Formation. In the HHPD model, the hydrate formation process is assumed to occur through adsorption of H_2 into the binary H_2–THF clathrate hydrate that is followed by diffusion of H_2 into empty S-cages in spherical particles of single crystals.[18] The resulting equation for the formation process is:

$$\frac{dn_{H_2}}{dt} = \frac{1}{\frac{1}{k_a A} + \frac{L}{D'_{H_2} A}} (f_{gas} - f_{eq}) \tag{1}$$

where n_{H_2} is the moles of H_2 included in the clathrate hydrate at time, t, and L, A, k_a, and D'_{H_2} represent the phase thickness of the H_2–THF clathrate hydrate, the area, the adsorption kinetic constant, and effective diffusion coefficient, respectively. The formation occurs according to the driving force between the fugacity, f, of the H_2 gas and that at equilibrium. The phase

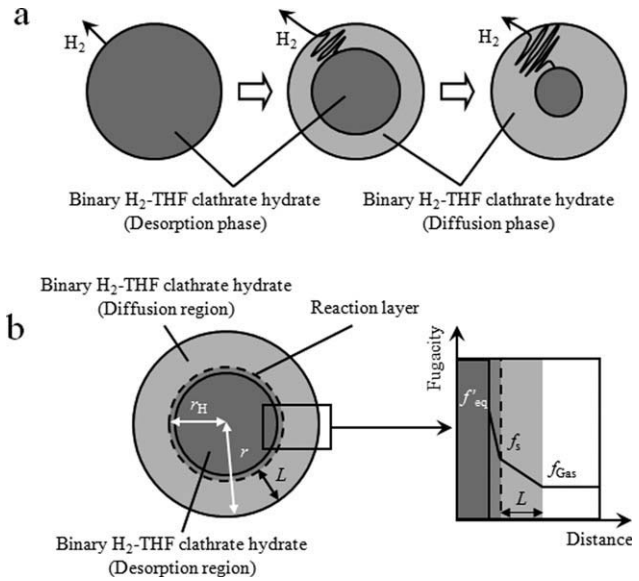

Figure 2. Hydrogen hydrate phase diffusion (HHPD) model for hydrate decomposition process.

(a) Conceptual diagram of the desorption and diffusion processes; (b) conceptual diagram of the desorption and diffusion phases and the correspond fugacity driving force.

thickness, L, is related to the H_2 occupancy in the clathrate hydrate and changes with time as does A.

Decomposition. The hydrate clathrate decomposition process was hypothesized to be reversible such that decomposition could be described by reversing the steps of the two-step formation process. Just as in the formation process, it was assumed that all particles were spherical and consisted of single crystals. In the binary H_2–THF clathrate hydrate, a single H_2 at most was assumed to be entrapped in an S-cage at the experimental conditions, as this is appropriate for the maximum pressures studied (ca. 10 MPa) and experimental evidence in the literature.[6]

Figure 2 shows a conceptual diagram of the hydrate clathrate decomposition process. In the first step, H_2 is desorbed from the binary H_2–THF clathrate S-cage and in the second step, H_2 diffuses through the hydrate phase to finally reach the bulk gas phase (Figure 2a). In the decomposition of the clathrate hydrate, it is assumed that there remains some H_2 in the hydrate phase even after decomposition goes to completion according to the equilibrium pressure or according to possible hysteresis. Therefore, it was assumed that there were different phases in the binary H_2–THF clathrate hydrate, namely a diffusion phase at the clathrate hydrate surface and a desorption phase on the interior of the clathrate hydrate particle (Figure 2b). In other words, diffusion, desorption, and bulk gas phases were assumed to exist for estimating the mass transfer that occurs. Each phase was described in terms of a fugacity driving force (Figure 2b). The HHPD model incorporates a desorption step in which the driving force for H_2 release is considered to be the difference between the H_2 fugacity at equilibrium conditions, f'_{eq}, and that at the reaction interface, f_s, multiplied by an area, A, and a desorption rate constant, k_{des} as follows:

$$\frac{dn_{H_2}}{dt} = k_{des}A\left(f'_{eq} - f_s\right) \tag{2}$$

At the initial stage of hydrate decomposition, A was calculated from the assumption of spherical particles as an average value after sieving, just as was done for the formation process. In this work, V_{hyd} was determined by assuming that it was proportional to the global occupancy, just as was assumed for the formation process as follows:

$$V_{hyd} = \frac{4}{3}\pi N(r-L)^2 \tag{3}$$

$$\frac{V_{hyd}}{V^i_{hyd}} = \frac{\theta_S - \theta_{eq,dec.}}{\theta_{eq,form.} - \theta_{eq,dec.}} \tag{4}$$

where L and V^i_{hyd} are the diffusion distance of hydrogen in H_2–THF clathrate hydrate diffusion phase and V_{hyd} at $L = 0$, respectively. The $\theta_{eq,from.}$ and $\theta_{eq,dec.}$ are equilibrium occupancies at formation and decomposition, respectively. To account for both formation and decomposition processes, the value of L was written in terms of the instantaneous occupancies as follows:

$$L = r - \left\{\frac{3V_{Hyd}}{4\pi N}\left(\frac{\theta_S - \theta_{eq.dec.}}{\theta_{eq.form.} - \theta_{eq,dec.}}\right)\right\}^{\frac{1}{3}} \tag{5}$$

The diffusion step of H_2 in hydrate phase, which is the driving force for H_2 migration, is considered to be the difference between the H_2 hydrate fugacity at the reaction interface, f_s, and bulk, f_{gas}, multiplied by an area and a mass transfer coefficient that depends on diffusion, k_{dif} as follows:

$$\frac{dn_{H_2}}{dt} = k_{dif}A\left(f_s - f_{gas}\right) \tag{6}$$

The k_{dif} was expressed as follows:

$$k_{dif} = \frac{D'_{H_2}}{L} \tag{7}$$

where D'_{H_2} is an effective diffusion coefficient of hydrogen in the H_2–THF clathrate hydrate diffusion layer that contains mass transfer contributions. This expression shows that the diffusion of H_2 in the clathrate hydrate becomes inhibited as the thickness of hydrate layer increases. Temperature dependence of the H_2 diffusivity is discussed later.

At quasi-equilibrium conditions, the left-hand side of Eq. 6 equals to that of Eq. 2, thus, Eq. 8 can be developed by eliminating the H_2 hydrate fugacity at the reaction interface:

$$\frac{dn_{H_2}}{dt} = \frac{1}{\frac{1}{k_{des}A} + \frac{L}{D'_{H_2}A}}\left(f'_{eq} - f_{gas}\right) \tag{8}$$

where the decomposition occurs according to driving force between the H_2 fugacity, f'_{eq}, at equilibrium and that of the gas phase, f_{gas}. We estimated the equilibrium fugacity to be the fugacity at long reaction time using Soave–Redlich–Kwong (SRK) equation of state.[20] Bulk fugacities were also estimated by the SRK equation of state.[20] The functional form of Eq. 8 is similar to that of Eq. 1. The HHPD model was used to correlate the experimental data using the absolute average deviation in moles as the objective function and using k_{des} and

Table 2. Fitted Parameters k_a and D'_{H2} for Hydrate Formation Process with the HHPD Model

Run	k_a [$\times 10^{-12}$ mol/(Pa/s/m^2)]	D'_{H2} [$\times 10^{-17}$ mol/(Pa/s/m)]	D_{H2} ($\times 10^{-12}$ m^2/s)	AAD ($\times 10^{-5}$ mol)
1	2.84 (±0.26)	9.49 (±1.7)	3.76 (±0.68)	3.56
2	3.98 (±0.68)	7.48 (±1.5)	3.88 (±1.20)	9.34
3	4.20 (±0.34)	8.95 (±1.5)	4.77 (±0.77)	7.64
4	3.74 (±0.34)	6.90 (±1.3)	3.47 (±0.63)	8.21
5	3.96 (±0.36)	8.86 (±1.6)	4.19 (±0.76)	3.62
6	2.43 (±0.22)	14.7 (±2.7)	4.20 (±0.76)	3.80
7	3.50 (±0.31)	8.00 (±1.5)	3.13 (±0.57)	4.26
8	3.26 (±0.30)	8.62 (±1.6)	3.67 (±0.67)	4.10

The values in parenthesis show variation in the parameters according to the lower or higher values of the particle size ranges given in Table 1.

D'_{H_2} as fitting parameters. Parameter sensitivity was examined by fitting the decay data in small time increments (ca. 1 h). As sieved particles give particle distributions, parameter variances were estimated by using low and high values of the sieved particle ranges for the hydrate formation process (Table 2) and the hydrate decomposition process (Table 3). Apparent diffusion coefficients, D_{H_2}, were estimated from the final slopes of the quasi-equilibrium data and the phase thickness of the model L for each temperature (Table 2). In the proposed phenomenological model, it is the intent of this work to capture features of the microscopic adsorption and diffusional processes with a small number of parameters that have physical meaning. The model uses the fugacity of the gas component as the driving force, which is common in other clathrate hydrate formation and decomposition models.[21–23]

Results and Discussion

Formation and decomposition of binary H_2–THF clathrate hydrate at three different temperatures are shown in Figures 3 and 4, respectively, along with the HHPD model correlations for formation (Eq. 1) and decomposition (Eq. 8). As shown in the Figures 3 and 4, the HHPD model could describe both formation and decomposition processes well and from the time scale of the processes, it is apparent that the formation process occurred more rapidly than the decomposition process. The model was applied to formation and decomposition experiments for which the initial pressure (Supporting Information, Figures S5–S7) and the particle sizes (Supporting Information, Figures S8 and S9) were varied. It was found that the model could suitably describe both the formation data (Table 2) and the decomposition data (Table 3). The trends of the model with the data clearly show that decomposition process was reversible and demonstrated consistency in the formation and decomposition processes. From the trend of the kinetic data, the process can be divided into at least two periods: one is a rapid reaction in the initial period and another is a slow reaction in the latter period. In our previous work,[18] the H_2 delocalization model taking into account of one reaction rate parameter (k) was examined; however, that model is unable to reproduce the experimental trends, especially for the rapid initial reactions. In the H_2 delocalization model, the assumptions of rapid diffusion and random reactions in the matrix are inappropriate according to the regression results. The present data exhibited particle size dependence on the hydrate formation and decomposition, which indicates that diffusion distance for H_2 should be taken into account into the model. Therefore, we chose two parameters (k and D') to fit using the H_2 hydrate phase diffusion model. The physical meaning of the two obtained parameters is discussed in the following section.

The rate parameters obtained in this work can be compared by determining the activation adsorption, desorption, and diffusion energies via:

$$k_a = k_a^* \times \exp(-\Delta E k_a / RT) \tag{9}$$

$$k_{dec} = k_{dec}^* \times \exp(-\Delta E k_{dec} / RT) \tag{10}$$

$$D'_{H2} = D^*_{H2} \times \exp(-\Delta E D'_{H_2} / RT) \tag{11}$$

where $\Delta E k_a$ is the activation energy for adsorption, $\Delta E k_{dec}$ is the activation energy for desorption, and $\Delta E D'_{H_2}$ is the activation energy for diffusion.

Figures 5 and 6 show the temperature dependence of the HHPD model parameters for formation and decomposition, respectively. The activation energies for adsorption and desorption ($\Delta E k_a$ and $\Delta E k_{dec}$) were found to be -28 and 24 kJ/mol, respectively. The negative value for adsorption indicates that the process is exothermic, which is usual for hydrate formation processes,[24] whereas the positive value for desorption shows that the process is endothermic. The absolute values between formation and decomposition processes,

Table 3. Fitted Parameters k_{des} and D'_{H2} for Hydrate Decomposition Process with the HHPD Model

Run	k_{des} [$\times 10^{-11}$ mol/(Pa/s/m^2)]*	D'_{H2} [$\times 10^{-17}$ mol/(Pa/s/m)]*	AAD ($\times 10^{-5}$ mol)
1	0.95 (±0.086)	6.99 (±0.64)	2.42
2	1.16 (±0.031)	6.22 (±2.26)	6.23
3*	–	–	–
4	1.00 (±0.090)	6.10 (±0.55)	4.88
5	0.71 (±0.065)	6.79 (±0.62)	3.07
6	1.46 (±0.133)	7.61 (±0.69)	2.66
7	1.07 (±0.098)	5.04 (±0.46)	2.97
8	0.69 (±0.063)	7.38 (±0.67)	2.93

The values in parenthesis show variation in the parameters according to the lower or higher values of the particle size ranges given in Table 1.
*Large particle size only used in formation experiments.

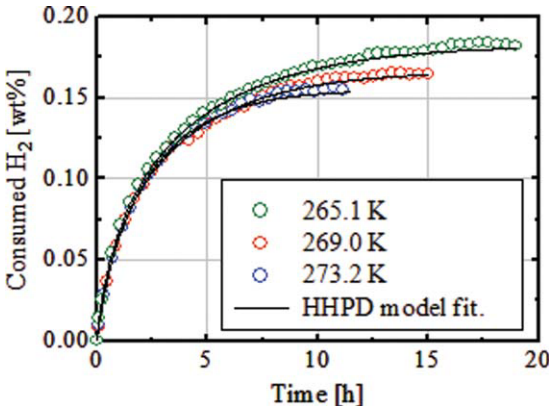

Figure 3. Hydrogen consumption by stoichiometric (19.06 wt %) THF clathrate hydrate particles as a function of time for an initial H_2 gas pressure of 5.0 MPa and a particle size range of 500–600 μm.

[Color figure can be viewed in the online issue, which is available at wileyonlinelibrary.com.]

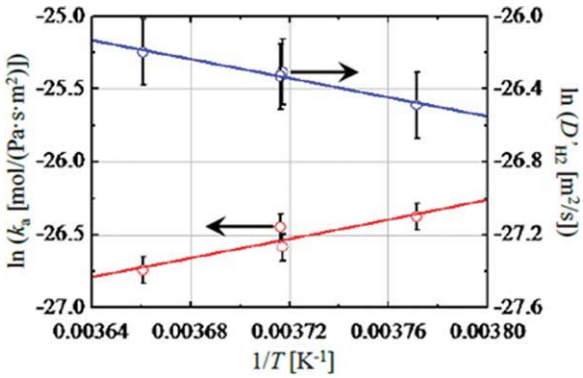

Figure 5. Arrhenius plot of adsorption parameter, k_a, of the HHPD model for hydrate formation from initial pressures of 5.0 MPa, particle sizes of stoichiometric THF hydrate of 500–600 μm.

[Color figure can be viewed in the online issue, which is available at wileyonlinelibrary.com.]

$|\Delta Ek_a|$ and $|\Delta Ek_{dec}|$ are comparable, suggesting that initial reactions were dominated by adsorption–desorption equilibrium. The absolute activation energy being higher than 20 kJ/mol generally seems to be chemical adsorption including rearrangement of water molecules rather than a simple physical adsorption. In other words, hydrate formation is exothermic that generates heat, which possibly promotes the rearrangement of water molecules or defects in the clathrate structure[25] one after the other. However, the explanation is less easy to rationalize for the reverse reaction (desorption process) because of the process being endothermic. On the other hand, the Joule–Thomson expansion of H_2 during the process must release heat and probably supplies some of the required energy for reversible water molecule and defect rearrangement. Such a thermal effect could explain some of the relatively large values of energy activation determined with the model that show the activation energy is on the order of H_2 bonding. Aspects of hydrate formation and decomposition processes are discussed in the following sections.

In an intermediate period between the initial reaction and the diffusion periods, there would seem to be a competitive stage in which both desorption and diffusion processes occur. Based on these observations, the fitted parameters could be determined from each dominant stage by considering the aforementioned times to further analyze the mechanism. The values of the diffusion coefficient were estimated by using the later portions of the H_2 consumption curves. The estimated diffusion coefficient values (D_{H_2}) are compared well with the literature[8] (Supporting Information, Figure S10). The D_{H_2} can be estimated in this work to be on the orders of 10^{-11} to 10^{-12} m^2/s, which were comparable with the results of NMR data by Okuchi et al., although our

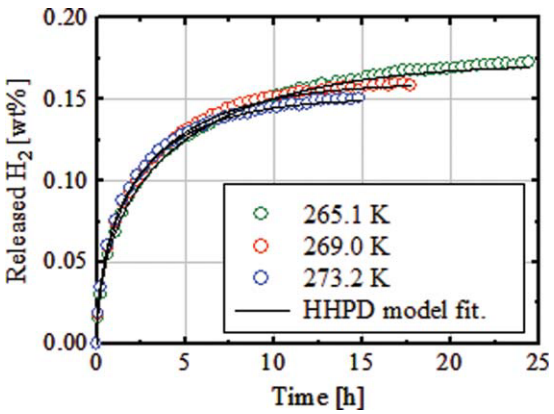

Figure 4. Hydrogen released from stoichiometric (19.06 wt %) THF clathrate hydrate particles as a function of time for a final H_2 gas pressure of 0.2 MPa and a particle size range of 500–600 μm.

[Color figure can be viewed in the online issue, which is available at wileyonlinelibrary.com.]

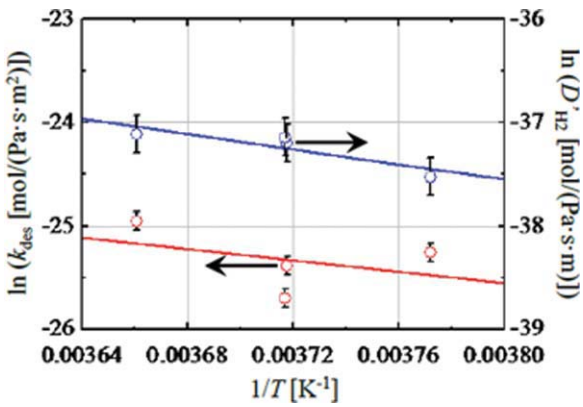

Figure 6. Arrhenius plot of desorption parameter, k_{des}, of the HHPD model for hydrate formation from initial pressures of 5.0 MPa, particle sizes of stoichiometric THF hydrate of 500–600 μm.

[Color figure can be viewed in the online issue, which is available at wileyonlinelibrary.com.]

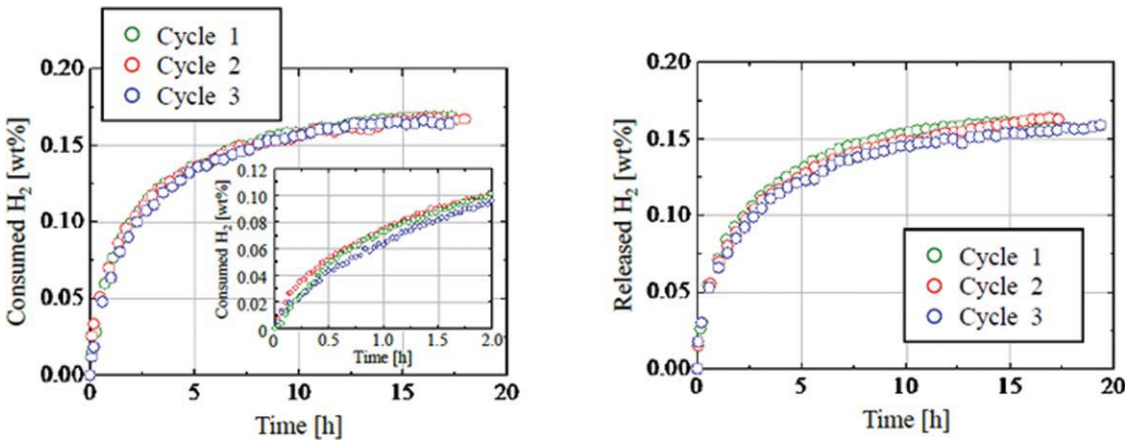

Figure 7. Time evolution of consumed and released H_2 from three successive H_2 clathrate hydrate formation and decomposition experiments at 269 K for particle sizes in the range of 500–600 μm, initial pressure of 5.0 MPa (P_{eq} = 4.9 MPa).

[Color figure can be viewed in the online issue, which is available at wileyonlinelibrary.com.]

values were higher than the values for diffusion through five-membered ring in the cage (10^{-14} to 10^{-16} m^2/s) reported by Mulder et al.[9] Frankcombe and Kroes[26] did not estimate the diffusion coefficient for five-membered ring diffusion on the time scale by MD simulations. Alavi and Ripmeester[27] also analyzed by MD simulation and their data for five-membered ring diffusion can be estimated to be on the order of 10^{-12} m^2/s from their plots, although the simulation conditions include H_2 inside double hydrate particles that are considerably different from the experimental conditions in this work.

Activation energies for diffusion ($\Delta ED'_{H_2}$) for formation and decomposition were determined to be 64 and 52 kJ/mol for the formation and decomposition processes, respectively. The absolute values between formation and decomposition processes are comparable, although the data variation was larger than the aforementioned values for ΔEk_a and ΔEk_{dec}. The experimental values reported by Okuchi et al.[8] based on NMR measurements show activation energy for diffusion to be 3 kJ/mol. Alavi and Ripmeester[27] determined values for the tunneling barrier of H_2 migration for two orientations by simulation with the assumption of the cage rigidity to be 99.1 and 118.9 kJ/mol for S-cage guests and 24.1 and 27.3 kJ/mol for L-cage guests. Frankcombe and Kroes[26] have reported by MD simulation that the activation energies for six-membered ring diffusion to be 32 $\pm$ 12 kJ/mol and that through five-membered ring to be more than 200 kJ/mol, respectively. Thus, H_2 migration into hydrate phase seems to require high activation energies as well as desorption (or adsorption) of H_2 in the S-cage. Activation energy for diffusion obtained in this work (52–64 kJ/mol) seems to be intermediate to those values reported for simulation methods. Coordination with rearrangement of water molecules, the temporal opening of a window, and the existence of hydrate clathrate defects[25] could possibly promote the H_2 diffusion during formation and decomposition.[9] Thermal effects due to microscopic Joule–Thomson expansion of the H_2 might be another effect. These possible phenomena cannot be distinguished between the adsorption and diffusion processes in the present model and will need microscopic studies with NMR, neutron diffraction, or simulations under similar conditions as those used in the experimental measurements to estimate their possibility.

Figure 7 shows the time evolution for three successive runs for conditions shown in Table 4 in which binary H_2–THF clathrate hydrates were formed and then decomposed. As shown in Figure 7, both the formation curves and the decomposition curves were very close, which is evidence for reversibility. On the other hand, there seemed to be a slight lowering of H_2 being released, which could possibly be attributed to small changes in the hydrate particles. From the HHPD model, it is possible to calculate the occupancies for three successive formation and decomposition cycles. As shown in Figure 8 for three successive cycles, the occupancies showed very similar trends in both formation and decomposition. The values fit using Eqs. 5 and 8 gave values of ($\theta_{eq,from.}$, $\theta_{eq,dec.}$) as (0.158, 0.0062), (0.156, 0.0031), and (0.155, 0.0063) for cycles 1, 2, and 3, respectively, indicating a slight decrease in the capacity of the clathrate hydrate for storing H_2 for successive loadings. Our calculation for the diminishing capacity for three recycles was 1.9% [=(0.158 $-$ 0.155)/0.158 $\times$ 100] and the reduction of the capacity was probably caused by indispensable vapor pressures of THF and water at each temperature. Nevertheless,

Table 4. Experimental Conditions Used to Study Recycles of Hydrogen–Tetrahydrofuran Clathrate Hydrates

Run	Cycle	W_{Hyd} (g)	d (μm)	$T_{form.}$ (K)	$T_{dec.}$ (K)	P_i (MPa)	P_{eq} (MPa)
9	1	7.30	500–600	269.1	269.0	5.03	4.88
10	2	7.30	500–600	269.1	269.1	5.01	4.87
11	3	7.30	500–600	269.1	269.1	5.01	4.88

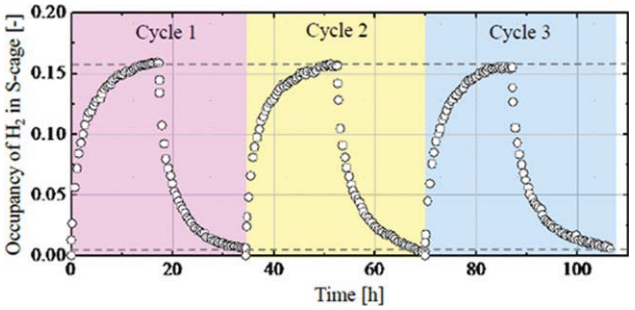

Figure 8. Calculated H_2 occupancies from successive H_2 clathrate hydrate formation and decomposition experiments at 269 K for particle sizes in the range of 500–600 μm, initial pressure of 5.0 MPa (P_{eq} = 4.9 MPa).

[Color figure can be viewed in the online issue, which is available at wileyonlinelibrary.com.]

the repetitive capacities are well within the uncertainties of the experiment and demonstrate that the formation and decomposition of H_2–THF hydrates are reversible and that recycle is possible at the conditions studied.

Conclusions

The H_2 hydrate phase diffusion model is applicable to both the formation and decomposition kinetics of H_2–THF clathrate hydrates. Formation of H_2–THF clathrate hydrates occurs in two steps via adsorption and diffusion, whereas decomposition of the clathrate hydrate occurs in two steps via desorption and diffusion. The formation and decomposition processes depend on temperature, pressure, and particle size of the clathrate hydrate. For a given temperature, pressure, and average particle size range conditions, the absolute activation energy for adsorption was higher than those for desorption, whereas the activation energy for diffusion was roughly comparable. Successive formation and decomposition experiments on H_2–THF clathrate hydrates with particle sizes in the range of 500–600 μm show that the process is reversible with no large change in hydrate structure.

Acknowledgments

The authors acknowledge the support of Monbukagakusho, Ministry of Education, Culture, Sports, Science, and Technology.

Literature Cited

1. Ogata K, Hashimoto S, Sugahara T, Moritoki M, Sato H, Ohgaki K. Storage capacity of hydrogen in tetrahydrofuran hydrate. *Chem Eng Sci*. 2008;63:5714.
2. Duarte ARC, Shariati A, Rovetto LJ, Peters CJ. Water cavities of sH clathrate hydrate stabilized by molecular hydrogen: phase equilibrium measurements. *J Phys Chem B*. 2008;112:1888–1889.
3. Strobel TA, Koh CA, Sloan ED. Hydrogen storage properties of clathrate hydrate materials. *Fluid Phase Equilib*. 2007;261:382–389.
4. Strobel TA, Kim Y, Andrews GS, Ferrell JR, Koh CA, Herring AM, Sloan ED. Chemical-clathrate hybrid hydrogen storage: storage in both guest and host. *J Am Chem Soc*. 2008;130:14975–14977.
5. Talyzin A. Feasibility of H_2-THF-H_2O clathrate hydrates for hydrogen storage applications. *Int J Hydrogen Energy*. 2008;33:111–115.
6. Strobel TA, Taylor CJ, Hester KC, Dec SF, Koh CA, Miller KT, Sloan ED. Molecular hydrogen storage in binary THF-H_2 clathrate hydrates. *J Phys Chem B*. 2006;110:17121–17125.
7. Lee H, Lee JW, Kim DY, Park J, Seo YT, Zeng H, Moudrakovski IL, Ratcliffe CI, Ripmeester JA. Tuning clathrate hydrates for hydrogen storage. *Nature*. 2005;434:743–746.
8. Okuchi T, Moudrakovski IL, Ripmeester JA. Efficient storage of hydrogen fuel into leaky cages of clathrate hydrate. *Appl Phys Lett*. 2007;91:171903–1–171903–3.
9. Mulder FM, Wagemaker M, van Eijck L, Kearley GJ. Hydrogen in porous tetrahydrofuran clathrate hydrate. *Chemphyschem*. 2008;9:1331–1337.
10. Senadheera L, Conradi MS. Rotation and diffusion of H_2 in hydrogen—ice clathrate by H-1 NMR. *J Phys Chem B*. 2007;111:12097–12102.
11. Senadheera L, Conradi MS. Hydrogen NMR of H_2-TDF-D_2O clathrate. *J Phys Chem B*. 2008;112:13695–13700.
12. Senadheera L, Conradi MS. Hydrogen nuclear spin relaxation in hydrogen-ice clathrate. *J Phys Chem A*. 2008;112:8303–8309.
13. Lee SY, Holder GD. Model for gas hydrate epuilibria using a variable reference chemical potential: part 1. *AIChE J*. 2002;48:161–167.
14. Martin A, Peters CJ. New thermodynamic model of equilibrium states of gas hydrates considering lattice distortion. *J Phys Chem C*. 2009;113:422–430.
15. Papadimitriou NI, Tsimpanogiannis IN, Papaioannou AT, Stubos AK. Evaluation of the hydrogen-storage capacity of pure H_2 and binary H_2-THF hydrates with Monte Carlo simulations. *J Phys Chem C*. 2008;112:10294–10302.
16. Alavi S, Ripmeester JA, Klug DD. Molecular-dynamics simulations of binary structure II hydrogen and tetrahydrofurane clathrates. *J Chem Phys*. 2006;125: art no. 014704.
17. Papadimitriou NI, Tsimpanogiannis IN, Stubos AK. Gas content of binary clathrate hydrates with promoters. *J Chem Phys*. 2009;131: art no. 044102.
18. Nagai Y, Yoshioka H, Ota M, Sato Y, Inomata H, Smith RL. Binary hydrogen-tetrahydrofuran clathrate hydrate formation kinetics and models. *AIChE J*. 2008;54:3007–3016.
19. Malegaonkar MB, Dholabhai PD, Bishnoi PR. Kinetics of carbon dioxide and methane hydrate formation. *Can J Chem Eng*. 1997;75:1090–1099.
20. Soave G. Equilibrium constants from a modified Redlich-Kwong equation of state. *Chem Eng Sci*. 1972;27:1197–1203.
21. Sean WY, Sato T, Yamasaki A, Kiyono F. CFD and experimental study on methane hydrate dissociation. Part I. Dissociation under water flow. *AIChE J*. 2007;53:262–274.
22. Sean WY, Sato T, Yamasaki A, Kiyono F. CFD and experimental study on methane hydrate dissociation. II. General cases. *AIChE J*. 2007;53:2148–2160.
23. Ota M, Abe Y, Watanabe M, Smith RL, Inomata H. Methane recovery from methane hydrate using pressurized CO_2. *Fluid Phase Equilib*. 2005;228:553–559.
24. Fujita S, Watanabe K, Mori YH. Clathrate-hydrate formation by water spraying onto a porous metal plate exuding a hydrophobic liquid coolant. *AIChE J*. 2009;55:1056–1064.
25. Koga K, Tanaka H. Rearrangement dynamics of the hydrogen-bonded network of clathrate hydrates encaging polar guest. *J Chem Phys*. 1996;104:263–272.
26. Frankcombe TJ, Kroes GJ. Molecular dynamics simulations of Type-sII hydrogen clathrate hydrate close to equilibrium conditions. *J Phys Chem C*. 2007;111:13044–13052.
27. Alavi S, Ripmeester JA. Hydrogen-gas migration through clathrate hydrate cages. *Angew Chem Int Ed*. 2007;46:6102–6105.

Manuscript received Oct. 25, 2009, and revision received Feb. 23, 2010.